

## Chapter 4

### Ekman layer transports, Ekman pumping, and the Sverdrup balance

Geostrophic flow, or the flow produced by a balance between the pressure gradient force and the Coriolis force, is frictionless flow. But momentum from the wind field is transferred into the ocean by friction; so frictional forces must be important in the surface boundary layer. The dynamics of this layer are best understood if it is assumed initially that the ocean interior is at rest, i.e. all isopycnal (and, as a consequence, all isobaric) surfaces are flat and steric height is constant everywhere. The balance of forces in the surface layer is then purely between the frictional force which transports momentum downwards, and the Coriolis force.

#### Ekman layer transports

The details of the flow in the surface layer, known as the Ekman drift after its first investigator, are complicated and depend on detailed knowledge of the coefficients of turbulent mixing. If fluctuations of periods shorter than a day are eliminated it is found that the current moves at an angle to the wind, turning further away from the wind direction and becoming weaker with depth. (Any of the text books mentioned in earlier chapters can be consulted for a description of the Ekman layer.) For the purpose of regional oceanography it is important to note that for a determination of total transport in the surface layer, knowledge about the details of the turbulent mixing process is not necessary. Theoretical analysis gives a relationship between the wind stress and the depth-integrated flow that develops in response to the wind which we formulate as

**Rule 3:** The wind-driven component of transport in the surface boundary or Ekman layer is directed perpendicular to the mean wind stress, to the left of the wind stress in the southern hemisphere and to the right in the northern hemisphere.

The magnitude of the Ekman layer transport  $M_e$  is given by:

$$|M_e| = |\boldsymbol{\tau} / f| . \quad (4.1)$$

Here,  $M_e$  is the wind-generated mass transport per unit width integrated over the depth of the Ekman layer, with dimensions  $\text{kg m}^{-1} \text{s}^{-1}$ ;  $\boldsymbol{\tau}$  is the wind stress, and  $f$  the Coriolis parameter introduced earlier. The unit width is measured across the transport direction, i.e. in the direction of the wind stress. The difference between the wind stress direction and the direction of  $M_e$  develops because the Coriolis force acts perpendicular to the water movement; Rule 3 ensures that it opposes the wind stress, and eqn (4.1) ensures that it balances it in magnitude.

If we now relax the initial assumption of flat isopycnal surfaces, a pressure gradient force will be present throughout the water column, up to the surface, and geostrophic flow will develop.  $M_e$  is then the additional, non-geostrophic transport in the Ekman layer. As with

our Rule 1 we note here again that our rules are not applicable near the equator, where according to eqn (4.1) Ekman layer transport grows beyond all bounds. In practical applications eqn (4.1) is valid to within about  $2^\circ$  of the equator, where quite large Ekman transports do occur in response to quite modest wind stresses.

### **Ekman pumping**

Wind-induced currents are among the strongest currents in the oceanic surface layer. More importantly, the depth-integrated Ekman transports rank among the most important causes of flow in the deeper layers as well, throughout the upper one or two kilometers of the ocean. This comes about because the Ekman transports converge in some regions and diverge in others, and vertical flow develops at the bottom of the surface boundary layer to replace or remove the converging water masses. This process of generation of flow below the surface layer through vertical movement into and out of it is known as Ekman pumping. Because of its importance for the distribution of hydrographic properties below the surface layer it is worth looking at this process in some detail.

We see from eqn (4.1) that variations of Ekman layer transport can result from two factors, the change of the Coriolis parameter with latitude and the structure of the wind stress field. In most situations the variation of  $f$  is small and Ekman pumping is dominated by spatial variations of wind stress. Figure 4.1 shows some examples. Between the Trades and the Westerlies (boxes *A* and *B*) the wind generates a mean flow into the box, resulting in Ekman pumping or downwelling. Poleward of the maximum Westerlies (box *C*) the net flow is directed outward, giving negative Ekman pumping ("Ekman suction") or upwelling. In all situations (except near the equator) the vertical velocity  $w$  at the base of the Ekman layer (positive for downwelling, negative for upwelling) is given by the divergence of the Ekman transport:  $-\rho_0 w = \partial M_e^x / \partial x + \partial M_e^y / \partial y$  where  $M_e^x$  and  $M_e^y$  are the components of  $M_e$  towards east and north respectively. From Rule 3 these components can be expressed, away from the equator, in terms of wind stress:

$$-\rho_0 w = \text{curl}(\boldsymbol{\tau}/f) = \partial(\tau_y/f)/\partial x - \partial(\tau_x/f)/\partial y \quad (4.2)$$

where  $\tau_x$  and  $\tau_y$  are the  $x$ - and  $y$ -components of  $\boldsymbol{\tau}$ . (The curl of a field of vectors is a vector which measures the tendency of the vectors to induce rotation. It has three components ( $\text{curl}_x$ ,  $\text{curl}_y$ , and  $\text{curl}_z$ ); but in oceanography only the third component which relates to rotation around the vertical is of interest, and the index  $z$  is never written. A visualization of the relationship between Ekman pumping and wind stress curl is shown in Figure 4.2). Fig 4.3 gives a map of the annual mean of  $\text{curl}(\boldsymbol{\tau}/f)$  for the world ocean. Most of the ocean is characterized by Ekman transport convergence or downwelling, indicated by an extensive region of negative  $\text{curl}(\boldsymbol{\tau}/f)$  from the tropics to the temperate zone. Positive  $\text{curl}(\boldsymbol{\tau}/f)$  or upwelling is found on the poleward side of the core of the Westerlies.

The basis of Figure 4.3 is eqn (4.2), which is not defined near the equator and along boundaries. What happens there can be understood if we return to the box models of Figure 4.1. The equatorial region (box *D*) is often characterized by upwelling: In the equatorial Atlantic and eastern Pacific Oceans winds are westward and fairly uniform; the change of sign of the Coriolis parameter across the equator produces Ekman transports of opposite signs at about  $2^\circ\text{N}$  and  $2^\circ\text{S}$ , i.e. Ekman suction and upwelling. Discussion of the situation in the equatorial Indian Ocean is left to Chapter 11 since it varies with the

monsoon. Along most eastern boundaries (box *E*) the wind stress is directed equatorward; Ekman transport is directed offshore but cannot come out of the coast - again, upwelling must occur. Near western boundaries the dynamics are governed by the western boundary currents; Ekman layer dynamics are often strongly modified, or negligible, in these regions.

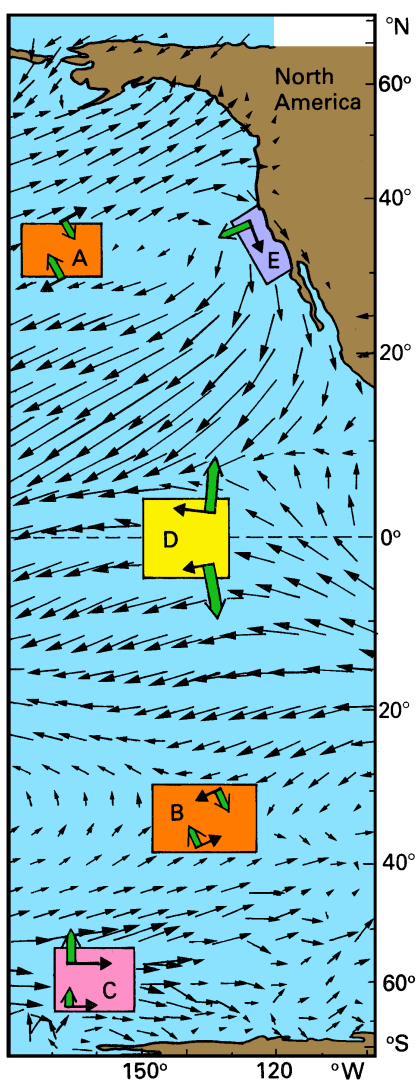


Fig. 4.1. Illustration of Ekman transport and Ekman pumping, based on the eastern Pacific Ocean. Full arrows indicate the wind, open arrows the Ekman transport resulting from the corresponding wind stress. Note the change of direction of the Ekman transport relative to the wind across the equator and the decrease of the Ekman transport, for equivalent wind stresses, with distance from the equator. Box *A* is between the Trade Winds and the Westerlies in the northern hemisphere; the Ekman transports at the northern and southern edges point into the box. The mean wind stresses along the east and west sides of the box do not add or subtract much to the transport budget. The result is net inflow into the box (convergence), or Ekman pumping and downwelling. Box *B* is the mirror image of *A* in the southern hemisphere; the Ekman transports are to the left of the wind, and there is again net inflow (convergence), or Ekman pumping and downwelling. Box *C* is located south of the maximum Westerlies; the Ekman transport is stronger at the northern edge than at the southern because the wind stress decreases towards the south. There is small net outflow (divergence), or Ekman suction and upwelling. Box *D* is on the equator. The winds stress does not vary much across the box, but the Coriolis parameter is small and changes sign across the equator, giving opposite directions for the Ekman transport north and south of the equator. The result is very large net outflow (divergence), or Ekman suction and upwelling. Box *E* is near an eastern coastline in the Trade Wind region. The wind stress is equatorward along the coast; the Ekman transport is directed offshore at the western edge but zero at the coast. The result is net outflow (divergence), or Ekman suction and upwelling.

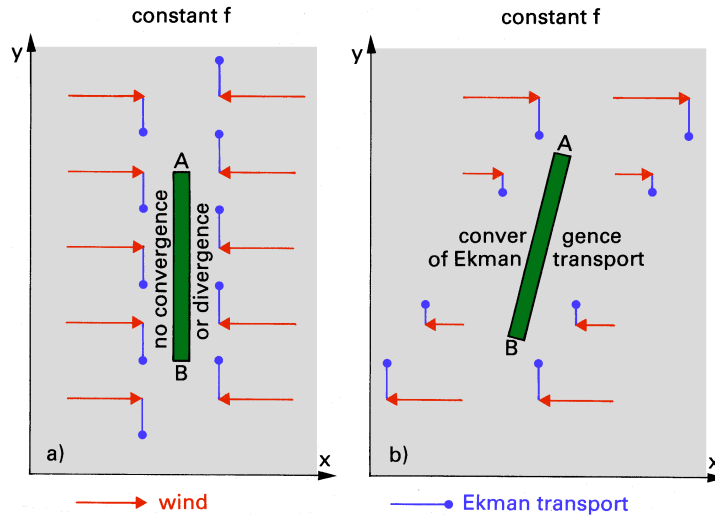


Fig. 4.2. A sketch of two wind fields and related Ekman transport, (a) with zero wind stress curl, (b) with non-zero wind stress curl. The tendency of the wind field to induce rotation can be visualized by the drifting balloon  $AB$ ; it does not rotate in (a) but rotates clockwise in (b). It is seen that Ekman pumping in the ocean occurs only where rotation is present in the atmosphere. (The variation of the Coriolis parameter has been neglected to simplify matters.)

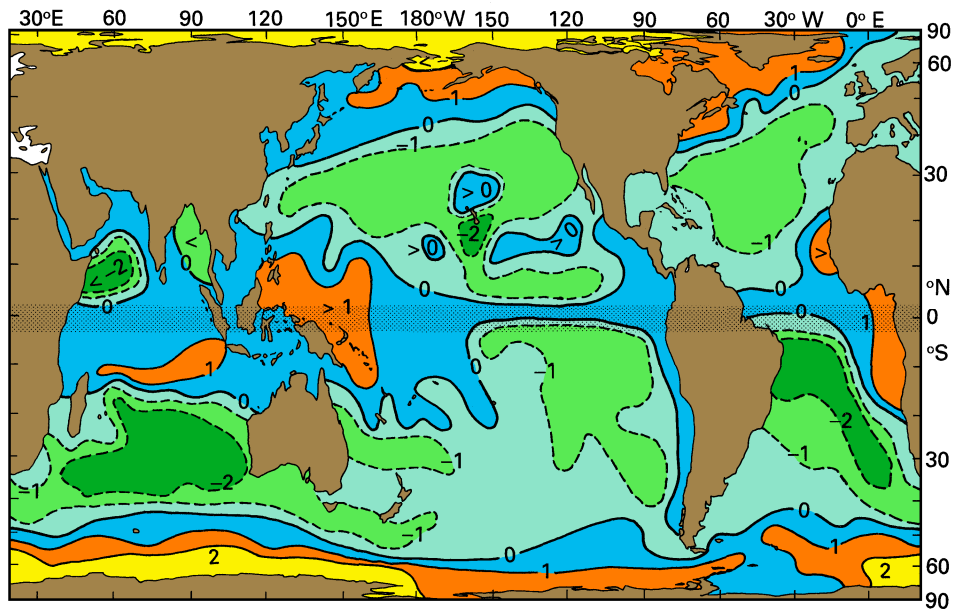


Fig. 4.3. Annual mean distribution of  $\text{curl}(\tau/f)$ , or Ekman pumping, calculated from the distribution of Fig. 1.4 ( $10^{-3} \text{ kg m}^{-2} \text{ s}^{-1}$ ). Positive numbers indicate upwelling. In the equatorial region ( $2^\circ\text{N} - 2^\circ\text{S}$ , shaded)  $\text{curl}(\tau/f)$  is not defined; the distribution in this region is inferred from the dynamical arguments of Fig. 4.1 and is not quantitative.

### The Sverdrup balance

We now return to the question raised at the end of the last chapter: What replenishes the bulges in the subtropical thermocline, seen (for example) in the temperature distribution of Fig 2.5 at 500 m depth? The answer is found by combining the dynamics of the ocean interior and western boundary currents with the dynamics of the Ekman layer.

It was shown in the last chapter that in the absence of forcing, thermocline bulges in a  $1^{1/2}$  layer ocean move westward at Rossby wave speed. We obtained an equation for the bulge movement, or local depth variation of the thermocline:

$$\partial H / \partial t = (\beta g / f^2(y)) (\Delta \rho / \rho_0) H \partial H / \partial x . \quad (4.3)$$

Bulge movement is a consequence of geostrophic transport convergence of anticyclonic eddies in the west and divergence in the east as shown in Figure 3.4, so eqn (4.3) can be seen as a balance equation for the convergence of the flow field. Now, the bulges seen in Figure 2.5c represent the annual mean, i.e. a steady state; so we must have  $\partial H / \partial t = 0$ . We achieve this by adding the convergence of the Ekman transport (Ekman pumping). The change in thermocline depth produced by Ekman pumping is the vertical velocity at the base of the Ekman layer. Taking this quantity from eqn (4.2) and adding it to eqn (4.3) gives the steady state balance as

$$(\beta g / f^2(y)) (\Delta \rho / \rho_0) H \partial H / \partial x = \text{curl}(\boldsymbol{\tau} / \rho_0 f) . \quad (4.4)$$

We can consider the right-hand side as continuously generating new bulges or depressions, which then migrate westwards as Rossby waves. The net effect is that in the steady state, an east-west gradient of  $H$  is set up which is in geostrophic balance, and that the mass divergence associated with this gradient matches the Ekman pumping convergence. The fact that energy propagates westward is no longer obvious in the steady state; but it does occur - the intense western boundary currents in each ocean are in fact dissipating the energy that has been fed into the ocean interior from the wind field by Ekman pumping. Because the energy which is fed into these narrow currents is the result of accumulation of energy from the wind field over the entire ocean surface, the western boundary currents are very intense, jet-like features. They achieve energy dissipation through bottom friction on the shelf and slope, and by spawning eddies and ejecting them into the open ocean.

Equation (4.4) is one form of an equation known as the *Sverdrup relation* for the  $1^{1/2}$  layer ocean. It was derived by Hans Ulrik Sverdrup and allows us to determine  $H$  everywhere for any ocean basin from a knowledge of  $H$  at its eastern boundary. (Knowledge of  $H$  at the western boundary is not of much use, since the Sverdrup relation includes only geostrophy and Ekman layer dynamics and does not apply to the western boundary currents.) We note that the right-hand side of eqn (4.4) is directly obtainable from the wind stress data. In other words, the depth variation of the thermocline, one of the key features of the oceans, can be determined from atmospheric observations alone! The left hand side of eqn (4.4), on the other hand, contains the essence of regional oceanography, namely the observations of temperature and salinity. In the  $1^{1/2}$  layer model which we used to simplify our description of ocean dynamics, the role of the observations is reduced to a determination of thermocline depth. In the more realistic case of a continuously stratified ocean the Sverdrup relation takes on the form (on multiplying both sides by  $f^2 / \beta$ )

$$g \partial P / \partial x = f^2 / \beta \operatorname{curl}(\boldsymbol{\tau} / \rho_0 f) \quad , \quad (4.5)$$

$$\text{where} \quad P(x,y) = \int_{z_0}^0 h(x,y,z) dz \quad (4.6)$$

has dimension  $\text{m}^2$  and is the depth-integral of the steric height  $h$  from an assumed depth of no motion  $z_0$  to the surface:  $\partial P / \partial x$  is the generalization of  $H(\Delta\rho/\rho_0)\partial H/\partial x$  in the  $1^{1/2}$  layer model. Note that (4.5) is well-defined at the equator. Evaluation of the right-hand side of eqn (4.5) gives, using  $\beta = df/dy$ ,

$$g \partial P / \partial x = f / (\beta \rho_0) \operatorname{curl}(\boldsymbol{\tau}) + \tau_x / \rho_0 \quad . \quad (4.7)$$

All three terms in eqn (4.7) are well-defined everywhere, including the equator. The spurious "infinite" speed of Rossby waves at the equator does not affect the steady state which those waves bring about.

In the form shown in eqn (4.5), both sides of the Sverdrup relation are completely well-defined by available data - the right-hand side comes from the annual mean wind stress shown in Figure 1.4, while the left-hand side comes from the annual mean density field derived from the data shown in Figure 2.5. This provides us with a powerful means for testing the validity of our concept of ocean dynamics. How well, then, do the two sides of the Sverdrup relation match one another?

Figure 4.4 shows a global map of depth-integrated steric height calculated from atmospheric data, i.e. using the right-hand side of the Sverdrup relation (eqn (4.5)) in combination with appropriate boundary conditions to ensure that no mass flux occurs through the eastern boundary (Godfrey, 1989). The same quantity is also shown in Figures 4.5 and 4.6, this time calculated from oceanographic information, i.e. based on the left hand side of eqn (4.5) for two different depths of no motion, 1500 m and 2500 m. General agreement between the results from both data sets is observed in the subtropics. All three diagrams show a maximum value of  $P$  near the western boundary of each ocean at  $30^\circ - 40^\circ$  N or S. The position of this maximum is well represented by Figure 4.4 in each basin. The number of contours from east to west in each ocean basin is fairly well represented, though the wind-based calculation produces a larger transport than the calculation based on ocean temperatures and salinities. This could be due, as has been suggested by researchers, to an inappropriately large choice of the constant  $C_d$  in the wind stress calculation of Hellerman and Rosenstein (1983).

It is also remarkable that over most of the oceans the choice of reference level for the integration of the oceanographic data fields does not influence the results very much. This indicates that flow between 1500 m and 2500 m depth is quite small, making both depths probably reasonably valid choices for a depth of no motion. Substantial differences between the strengths of the flows predicted by Figures 4.5 and 4.6 occur in the Antarctic region, indicating that at these latitudes substantial flow occurs below the 1500 m level. This aspect of the circulation will be discussed in detail in Chapter 6.

A major failing of the calculation from atmospheric data occurs west of the southern end of Africa, where it shows very strong north-south gradients of  $P$ . These gradients imply an intense geostrophic flow across the South Atlantic Ocean to South America, which then

flows about 500 km southward and returns to the Indian Ocean. In reality, such intense flows which pass through an open ocean region are unstable, particularly when they "double back" on themselves as in Figure 4.4 southwest of South Africa; the real Agulhas Current outflow turns eastward to join the Antarctic Circumpolar Current, as seen in Figures 4.5 and 4.6. The chapters on the Indian Ocean will take this up further.

The outflows from the western boundary currents of the North Atlantic and North Pacific Oceans are also not well represented by the model derived from the wind data. Both are underestimated in magnitude; and the Gulf Stream separation occurs near Labrador, rather than at its observed location near Cape Hatteras in the northern USA. However, considering the simplicity of the concept of Ekman pumping, Rossby wave propagation, and the Sverdrup balance as the result of an equilibrium between these two phenomena, it is pleasing to see to what large degree the atmospheric and oceanographic data sets available today confirm its validity. The model certainly accounts for a considerable fraction of what we see in the depth-integrated flow of the world ocean. The plan for the World Ocean Circulation Experiment (Figure 2.4) is therefore based on the concept that a systematic survey of temperature and salinity, augmented by direct current measurements through moorings in regions where the Sverdrup relation does not hold, will result in a reliable description of the oceanic circulation.

### The stream function and depth-integrated transports

Without doubt, depth-integrated steric height  $P$  is the best quantity to test the Sverdrup relation. Unfortunately, it does not provide the most convenient visualization of the flow field on oceanic scales, since its distribution combines variations of depth-integrated flow with the latitude-dependence of the Coriolis parameter. A better representation is achieved by introduction of a stream function which eliminates  $f$  from the picture. The direction of the total net transport between the assumed depth of no motion and the surface is then indicated by the direction of the streamlines, and its magnitude is inversely proportional to the distance between them. Because there cannot be any flow through the coast, coastlines are streamlines by definition. If the coast is continuous it coincides with a single streamline, i.e. the value of the stream function along the coast is the same. It is also possible to estimate the flow around major islands such as Australia and New Zealand and allocate stream function values to their coasts (Godfrey, 1989).

If we neglect the small flow from the Arctic into the north Pacific Ocean and consider Bering Strait closed, the world ocean is surrounded by a single continuous coastline (formed by the Asian, African and American continents) and contains only few large islands (Antarctica, Greenland, Iceland, Australia, New Zealand, Madagascar). Figure 4.7 shows the volume transport stream function for this continuous domain. Since the stream function calculation is based on Sverdrup dynamics it can only proceed starting from eastern boundaries and extend to the outer edges of the western boundary currents. The differences in stream function values across the gap near the western coastlines give the transport of the western boundary currents. Details of the depth-integrated flow near the equator that are masked in Figure 4.4 by the variation of the Coriolis parameter (in particular the sign change of  $f$  across the equator) come out clearly in the stream function map. The North Equatorial Countercurrent, flowing eastward between  $5^\circ$  and  $15^\circ\text{N}$  in the North Pacific Ocean, is seen as a major feature. The corresponding feature in the South Pacific Ocean is extremely weak and restricted to an area south-east of Papua New Guinea. A strong counter-

current is seen in the southern Indian Ocean. This asymmetrical distribution of currents reflects similar asymmetries of the annual mean wind stress field of Figure 1.4.

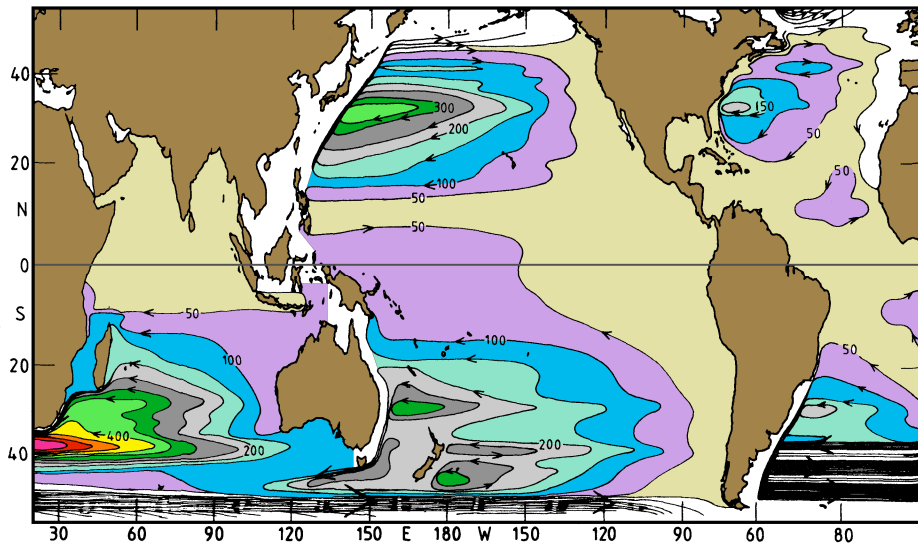


Fig. 4.4. Depth-integrated steric height  $P$ , calculated from the right-hand side of the Sverdrup relation (eqn (4.5)), using the data from Hellerman and Rosenstein (1983). Units are  $10^1 \text{ m}^2$ . For details of the integration procedure see Godfrey (1989).

An important thing to note for later reference is the magnitude of the western boundary currents generated by the Sverdrup mechanism: 50 Sv for the Kuroshio, 30 Sv for the Gulf Stream and the Brazil Current, 25 Sv for the East Australian Current, and 70 Sv for the Agulhas Current; independent estimates of the flow between Australia and Indonesia of 16 Sv were used for obtaining the latter two transports. To give some feeling what these numbers mean we note that 50 Sv correspond to about 4000 cubic kilometers per day! When it comes to the discussion of individual oceans it will become clear that none of these transport estimates is very accurate, because regional effects modify the boundary currents. Nevertheless, there can be no doubt that the currents are wind-driven, in the sense that they provide continuity of transport for the Sverdrup regime of the ocean interior.

Another feature of Figure 4.7 worth noting is the existence, in each ocean basin, of circulations bounded by contours of zero stream function value. The circulation cells bounded by zero stream function contours are known as "gyres"; those lying between the maximum westerlies and Trades in Figure 4.7 are known as the *subtropical gyres*. Within each subtropical gyre, the wind stress curl generates equatorward depth-integrated flow in the ocean interior, which returns poleward in the western boundary currents. Poleward of the subtropical gyres in the Northern Hemisphere are the *subpolar gyres*. Flow within these is poleward in the interior and equatorward at the western boundary. The convergence of the western boundary currents of the subtropical and subpolar gyres produces the *polar fronts*, regions of strong horizontal temperature and salinity gradients where warm subtropical

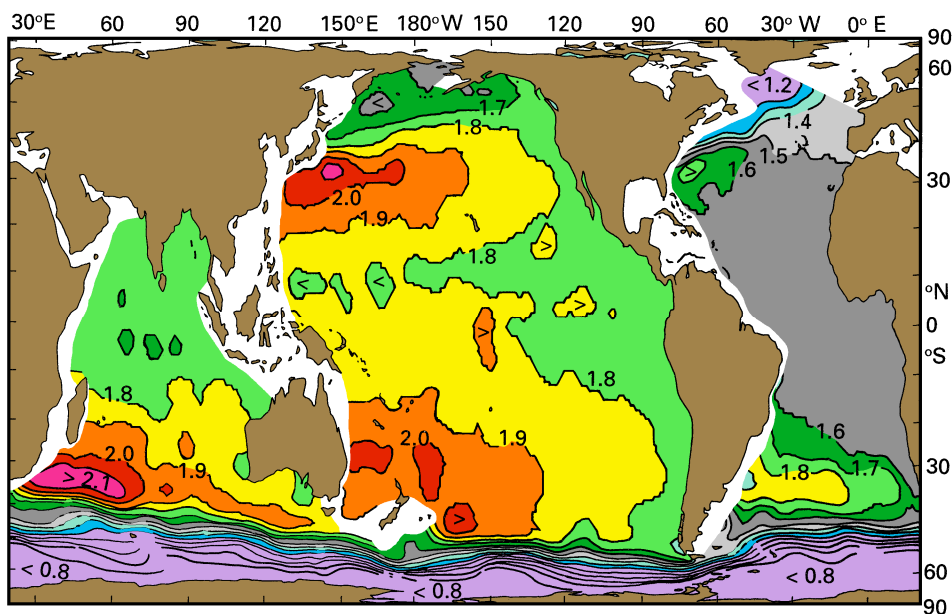


Fig. 4.5. Depth-integrated steric height  $P$ , from the left side of the Sverdrup relation (eqn (4.5)), using the data from Levitus (1982), for a depth of no motion of 1500 m. Units are  $10^3 \text{ m}^2$ .

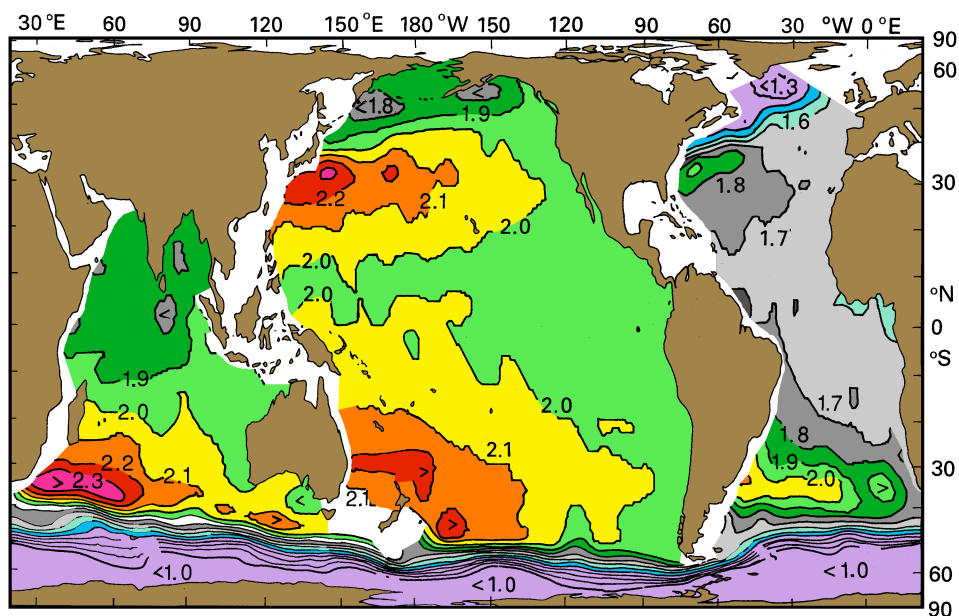


Fig. 4.6. Depth-integrated steric height  $P$ , from the left side of the Sverdrup relation (eqn (4.5)), using the data from Levitus (1982) for a depth of no motion of 2500 m. Units are  $10^3 \text{ m}^2$ .

water meets cold subpolar water along the zero streamline contour (compare Figure 2.5). Further gyres are evident between 15°N and 10°S; they form part of the complex equatorial current system which will be discussed in later chapters and are not usually recognized as gyres by name.

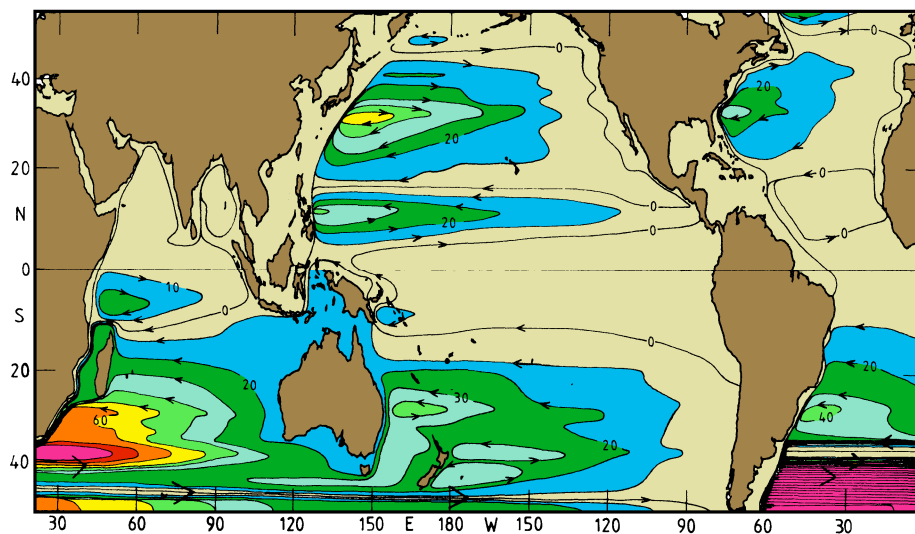


Fig. 4.7. Stream function for the world ocean, calculated from the wind stress data of Hellerman and Rosenstein (1983). Contour interval is 10 Sv.

It can be shown that if the winds were purely zonal and did not vary with longitude, the zero stream function contours would coincide with zero contours of wind stress curl. In other words, subject to the same assumptions, the boundaries of the gyres would coincide with the maximum westerly wind stresses, and with the maximum Trades. Purely zonal winds with no longitudinal variation are of course a somewhat poor description of the real mean winds; but the assumption is useful as a first approximation. The lines of zero stream function in Figure 4.7 do indeed either lie close to the maximum westerlies, or the maximum Trades, as can be seen by comparison with Figure 1.2.

Since the depth-integrated flow cannot cross streamlines, there is no *net* transport of mass between adjacent gyres (provided, that is, that the conditions of the Sverdrup circulation are met). This does not mean, however, that no water crosses from one gyre into another. In fact, transport in the surface layer across zero streamlines is maximum because the zonal wind stresses along these boundaries - and as a consequence the Ekman transport - are at a maximum. The surface layer transport is balanced by geostrophic transport below, so the *net* transport is zero. At the equatorward boundary of the subtropical gyres the Ekman transport is directed poleward and moves warm water away from the tropics, while the compensating deep geostrophic flow brings cold water into the tropics. Thus, although there is no net mass transport across the zero stream function contour, there is substantial

poleward transport of heat. To give an example, a simple calculation with the winds of Figure 1.2 shows that in the north Pacific Ocean the northward Ekman transport across the southern edge of the subtropical gyre at about 16°N (the position of the strongest Trades) amounts to some 28 Sv, with equal and opposite (and colder) geostrophic flow below. Similarly, there is a net poleward Ekman flux of 29 Sv across the northern edge of the south Pacific subtropical gyre at about 14°S, again compensated by equal and opposite geostrophic flow of lower mean temperature, so that heat is transported poleward here also. Thus the simple wind-driven circulation of Figure 4.7 which gives such a good illustration of the use of Sverdrup dynamics can be very misleading when it comes to a discussion of the amount of heat carried by the ocean.

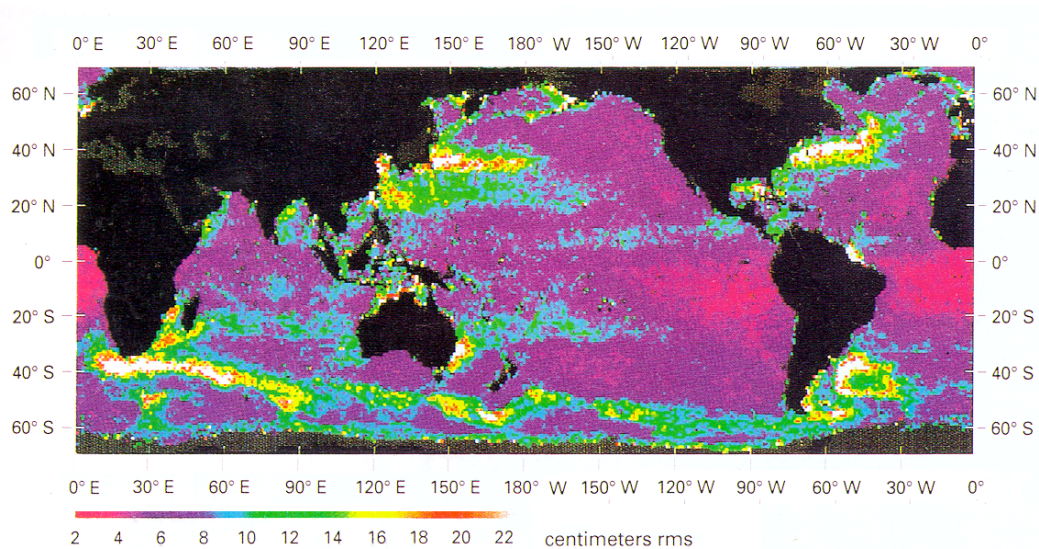


Fig. 4.8. Annual mean of eddy energy in the ocean as observed by satellite altimeter during December 1986 – November 1987. The eddies are detected by measuring the shape of the sea surface, which bulges downward in cyclonic and upward in anticyclonic eddies as explained in Figures 2.7 and 3.3. The quantity shown is the standard deviation of observed sea level (cm) from the mean sea level over the observation period. From Fu *et al.* (1988).

This concludes our discussion of ocean transport dynamics. A legitimate question at this point could be: If we go out to sea on a research vessel and make some observations, to which degree can we expect to see our picture of the large oceanic gyres and associated currents confirmed by the new data? A first answer is of course that Figures 4.5 and 4.6 are based on observations; they should therefore reflect the real world. A second answer is that they are based on annual mean data distributions. The question is then, can we expect to find the annual mean situation if we go out to sea and take a snap shot of the temperature and salinity distribution?

The answer is - yes, if we make our study area large enough. A synoptic survey of the subtropical north Atlantic Ocean would show the subtropical gyre. However, superimposed we would find a wealth of other structures, mainly eddies of all shapes and sizes. If we restricted our survey to a square of some 200 km base length we could find it very difficult

to recognize the mean flow. The water in the ocean is constantly mixed, a major mixing mechanism being eddy mixing. Figure 4.8 shows mean eddy energy in the ocean. The western boundary currents (Gulf Stream, Brazil Current, Kuroshio, East Australian Current, Agulhas Current) and the Circumpolar Current stand out as regions of particularly high eddy energy. Eddies in these regions are so energetic that the associated currents can reverse the direction of flow. In the western boundary currents they turn the water movement from poleward to equatorward; poleward mean flow is only observed if the study area is larger than the typical eddy size, which is of the order of 200 km diameter. Away from the boundary currents eddy energy goes down rapidly; but annual mean velocities decrease as well, and eddies can still reverse the observed direction of mean flow if the study area is too small. Figure 4.9 demonstrates this for the area of the Azores Current in the eastern north Atlantic Ocean. In the example the cruise covered an area of roughly  $550 \cdot 550$  km with 86 stations. At least three eddies are seen, but the Azores Current is still visible meandering through the region between the eddies. A smaller study area would not show much resemblance between the annual mean and the actual situation.

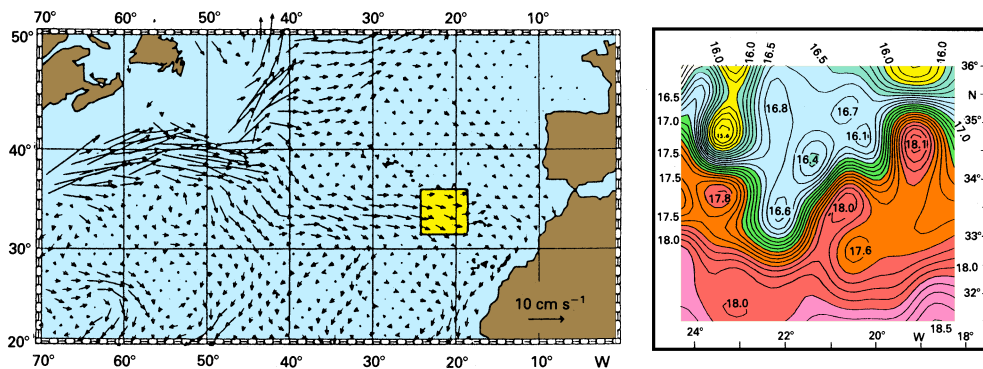


Fig. 4.9. Eddies in the Azores Current. (a) Mean surface flow based on historical data. (b) The box of panel (a) enlarged, showing the Azores Current and eddies as indicated by the temperature of the surface mixed layer, during April 1982. (Horizontal temperature gradients indicate a sloping interface and associated eddies in the manner of Fig. 3.3.) From Käse *et al.* (1985).